

\mathcal{PT} -symmetric Feedback Induced Linewidth Narrowing

Yuanjiang Tang¹, Chao Liang¹, Xin Wen¹, Weipeng Li¹, An-Ning Xu¹ and Yong-Chun Liu^{1,2*}

¹State Key Laboratory of Low-Dimensional Quantum Physics,

Department of Physics, Tsinghua University, Beijing 100084, China and

²Frontier Science Center for Quantum Information, Beijing 100084, China

(Dated: May 18, 2023)

Narrow linewidth is a long-pursuing goal in precision measurement and sensing. We propose a parity-time symmetric (\mathcal{PT} -symmetric) feedback method to narrow the linewidths of resonance systems. By using a quadrature measurement-feedback loop, we transform a dissipative resonance system into a \mathcal{PT} -symmetric system. Unlike the conventional \mathcal{PT} -symmetric systems that typically require two or more modes, here the \mathcal{PT} -symmetric feedback system contains only a single resonance mode, which greatly extends the scope of applications. The method enables remarkable linewidth narrowing and enhancement of measurement sensitivity. We illustrate the concept in a thermal ensemble of atoms, achieving a 48-fold narrowing of the magnetic resonance linewidth. By applying the method in magnetometry, we realize a 22-times improvement of the measurement sensitivity. This work opens the avenue for studying non-Hermitian physics and high-precision measurements in resonance systems with feedback.

Linewidth is one of the key factors that determine the performance of resonance systems, such as atoms, optical cavities and mechanical resonators. Especially, for precision measurement and sensing, we always strive for a narrow linewidth to achieve better measurement sensitivity. In various precision experiments such as atomic magnetometry [1, 2], atomic gyroscope [3], nuclear magnetic resonance spectroscopy [4], exploration of dark matter [5, 6] and exotic forces [7], a very narrow linewidth enables one to detect extremely weak signals. On the other hand, narrow linewidth also represents long coherence time, which is beneficial for quantum storage and quantum information processing. In order to reduce the linewidth, various methods have been proposed, e.g., antirelaxation coating of vessel walls [8–10], the spin-exchange-relaxation-free mechanism [11, 12], the nonlinear magneto-optical rotation approach [13] and the coherent population trapping scheme [14] in atomic systems. However, these methods typically have specific and stringent requirements, e.g., highly demanding fabrication, strict magnetic shielding or specific energy levels.

In recent years, parity-time (\mathcal{PT}) symmetry has attracted much interest, inspired by its unique property of exhibiting real energy spectra with non-Hermitian Hamiltonians [15–18]. Much progress has been made in different systems, including optics [19–25], atoms [26–29], electronics [30–32], nitrogen-vacancy centers [33], optomechanics [34–38], acoustics [39, 40], and microwave systems [41], with potential in sensing [42–46]. The study of \mathcal{PT} symmetry provides a powerful tool of engineering gain and loss and controlling the system linewidth. However, previous realizations of \mathcal{PT} symmetry required two or more modes, which is not applicable in a large variety of systems that contain only a single resonance mode.

In this work we realize a novel type of \mathcal{PT} -symmetric system by using a single resonance mode, which leads to efficient and tunable linewidth narrowing. First, the

effective gain is realized by introducing feedback. Feedback is a fundamental component of modern control theory [47], and has been widely employed in quantum systems [48] with applications in laser cooling [49–64], phase transition [65–70], quantum state preparation [71–78], quantum dynamical control [79–86], nonlinearity generation [87–91], and quantum amplification [92, 93] as well as generation of squeezing [94–97] and entanglement [98–101]. Here we make use of positive feedback to transform loss into gain. Second, we design a measurement-feedback loop in which the two quadrature components are controlled separately, which breaks the symmetry between the quadratures, so that the two quadratures of a single resonance mode behave like two different modes with gain and loss, and the parity operation represents the interchange between the two quadratures of the same mode. Therefore, unlike the conventional \mathcal{PT} -symmetric systems that typically contain two or more modes, here the \mathcal{PT} -symmetric feedback system requires only a single resonance mode, which greatly extends the application of \mathcal{PT} symmetry in a diversity of single resonance systems. Such a method shows great advantage in linewidth narrowing and sensitivity enhancement. Using an experimental setup with a thermal atomic ensemble, we observe a 48-fold narrowing of the magnetic resonance linewidth, and achieve a 22-times improvement of the measurement sensitivity for magnetometry.

We consider a generic dissipative resonance system, which can be described by the Hamiltonian $H = \omega_0 a^\dagger a$ and the corresponding quantum Langevin equation $\dot{a} = (-i\omega_0 - \kappa)a - \sqrt{2\kappa}a_{\text{in}}$, where a (a^\dagger) is the annihilation (creation) operator of the resonance mode, ω_0 is the resonance frequency, κ is the amplitude dissipation rate with the associate noise operator being a_{in} . The quadratures of the resonance mode are defined as $X = (a + a^\dagger)/2$ and $Y = i(a^\dagger - a)/2$, which correspond to the bases in the phase space. X_{in} and Y_{in} correspond to the

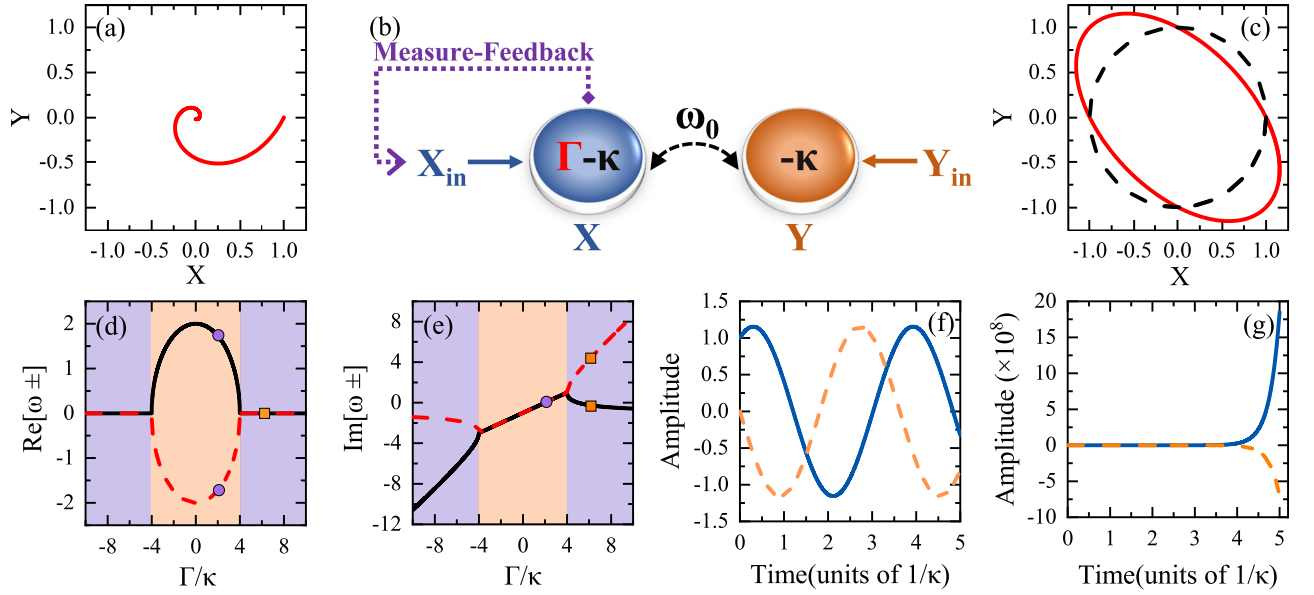


FIG. 1. (a) Typical trajectory of a dissipative resonance system in the phase space. (b) Schematic diagram of the \mathcal{PT} -symmetric feedback system. (c) Phase-space trajectory of the \mathcal{PT} -symmetric feedback system (red solid curve) and Hermitian resonance system (black dashed curve). (d),(e) Real and imaginary parts of the eigenvalues for Γ/κ varied from -10 to 10 and $\omega_0/\kappa = 2$. The purple dots represent the case of $\Gamma = 2\kappa$, and the orange squares represent the case of $\Gamma = 6\kappa$, which are the eigenvalues of Figs.1(f) and (g), respectively. (f),(g) Typical time evolution of quadratures X (blue solid curve) and Y (orange dashed curve) in \mathcal{PT} -symmetric phase ($|\Gamma| < 2\omega_0$) and symmetry-broken phase ($|\Gamma| > 2\omega_0$).

input quadratures. The equations of motion for the quadratures are given by $\dot{X} = -\kappa X + \omega_0 Y - \sqrt{2\kappa} X_{\text{in}}$, $\dot{Y} = -\kappa Y - \omega_0 X - \sqrt{2\kappa} Y_{\text{in}}$. Because of the dissipation, the evolution trajectory in the phase space is a spiral curve approaching the origin of coordinates, as shown in Fig. 1(a). To construct a \mathcal{PT} -symmetric Hamiltonian, as sketched in Fig. 1(b), we use a feedback loop in which X component is measured with the outcome feedback to input X_{in} component, i.e., $X_{\text{in}} \rightarrow X_{\text{in}} - \Gamma X/\sqrt{2\kappa}$, with Γ being the feedback parameter. Then the system dynamics is modified as

$$\begin{cases} \dot{X} = (\Gamma - \kappa) X + \omega_0 Y - \sqrt{2\kappa} X_{\text{in}}, \\ \dot{Y} = -\kappa Y - \omega_0 X - \sqrt{2\kappa} Y_{\text{in}}. \end{cases} \quad (1)$$

In the bases of quadratures with the vector $\Psi = (X \ Y)^T$, the equations can be rewritten as $\dot{\Psi} = -iH_{\text{eff}}\Psi$ with

$$H_{\text{eff}} = \begin{pmatrix} i\frac{\Gamma}{2} & i\omega_0 \\ -i\omega_0 & -i\frac{\Gamma}{2} \end{pmatrix} + i\left(\frac{\Gamma}{2} - \kappa\right) \mathbf{I}, \quad (2)$$

where \mathbf{I} is the identity matrix. After dropping the identity matrix term that corresponds to a common gain or loss, the effective Hamiltonian is \mathcal{PT} -symmetric. Here the parity operator \mathcal{P} is the Pauli operator σ_x representing the interchange between the two quadratures, and the time-reversal operator \mathcal{T} denotes complex conjugation operation. Therefore, the feedback transfers the dissipative resonance system into a \mathcal{PT} -symmetric system, with equal gain and loss in two quadratures of the

same resonance mode. The key point is that the feedback breaks the symmetry between the quadratures, and thus the two quadratures of a single resonance mode behave like two different modes with gain and loss. As shown in Fig. 1(b), the effective coupling strength between the quadratures is equal to the resonance frequency ω_0 , as it is just the energy exchange frequency for different components within the system.

For the Hermitian case without dissipation, the trajectory in the phase space is a closed circle. However, in the \mathcal{PT} -symmetric case, the trajectory is squeezed into an oblique ellipse, as plotted in Fig. 1(c). In this case, the total effect of gain and loss for the $\pm\pi/4$ quadratures $X_{\pm} = (X \pm Y)/\sqrt{2}$ are balanced, but the couplings between X_+ and X_- are rescaled as a result of gain and loss, with $\dot{X}_+ = -(\omega_0 - \Gamma/2)X_-$ and $\dot{X}_- = (\omega_0 + \Gamma/2)X_+$. Therefore, the trajectory along $\pm\pi/4$ direction is squeezed (stretched) by a factor of $1 \pm \Gamma/(2\omega_0)$, resulting in an ellipse with an oblique angle of $\pi/4$.

The resultant \mathcal{PT} -symmetric system possesses both \mathcal{PT} -symmetric and \mathcal{PT} -symmetry-broken phases, which can be tuned by the feedback parameter Γ . The eigenvalues of H_{eff} are $\omega_{\pm} = i(\Gamma/2 - \kappa) \pm \sqrt{\omega_0^2 - \Gamma^2/4}$, whose real (imaginary) parts represent the resonance frequency (dissipation rate) of the eigenmodes. In Fig. 1(d) and (e) we plot the real and imaginary parts of the eigenvalues as functions of feedback parameter Γ . When the feedback is weak ($|\Gamma| < 2\omega_0$), the real parts of the eigenvalues are opposite to each other while the imaginary parts are equal,

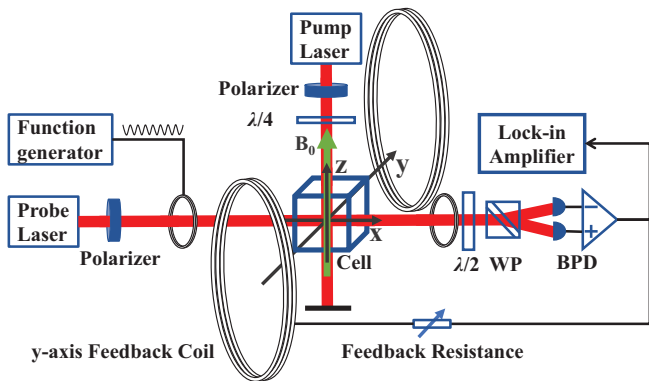


FIG. 2. Experimental setup with a thermal atomic ensemble. A 1 cm^3 cube glass cell is rich in ^{133}Cs , filled with 600 Torr ^4He and 20 Torr N_2 and heated to $100\text{ }^\circ\text{C}$. The linearly polarized probe laser power is $25\text{ }\mu\text{W}$ and frequency is 40 GHz below the $F = 4$ to $F' = 2$ transition of the ^{133}Cs D_2 line. The circularly polarized pump laser power is 1 mW and frequency is the $F = 4$ to $F' = 3$ transition of the ^{133}Cs D_1 line. B_0 , z -axis static magnetic field, $\lambda/4$, quarter wave plate; $\lambda/2$, half wave plate; WP, Wollaston prism; BPD, balanced photodetector. The output signal of the BPD is applied to a loop consisting of a feedback resistor and a y -axis feedback coil to achieve magnetic field feedback. The function generator is used to generate the weak driving magnetic field B_x .

and the system is in the \mathcal{PT} -symmetric phase. In this case the time evolutions of the quadratures X and Y are still trigonometric functions, but the phase difference is no longer $\pi/2$ [Fig. 1(f)], which is a result of the phase advance or lag induced by the effective gain or loss. If the feedback is strong enough ($|\Gamma| > 2\omega_0$), the eigenvalues are purely imaginary, indicating that the eigenmodes are no longer harmonic modes. Then the amplitude of the quadratures increases exponentially with time, as shown in Fig. 1(g).

We demonstrate the \mathcal{PT} -symmetric feedback mechanism in a thermal atomic ensemble, which is a typical example of magnetic resonance system. The experimental setup is sketched in Fig. 2. A ensemble of thermal cesium atoms is filled in a vapor cell, and the atoms can be described by a collective spin with spin polarization $\mathbf{P} = (P_x, P_y, P_z)$, where $P_{\mu=x,y,z}$ is the spin polarization component along μ axis. A beam of circularly polarized laser propagating along the $-z$ direction optically pumps the atomic ensemble to polarize the collective spin. A static magnetic field of $B_0 = 2.2\text{ }\mu\text{T}$ is applied along z axis, then the collective spin undergoes a Larmor precession around z axis, with Larmor frequency being $\omega_0 = \gamma B_0$, where γ is the gyromagnetic ratio of the atom. Thus, the transverse components $P_{x,y}$ oscillates in the xy plane, constituting a harmonic oscillator. We measure the spin polarization component P_x using a probe laser via polarization homodyne detection, and the output signal is then fed into a loop that includes

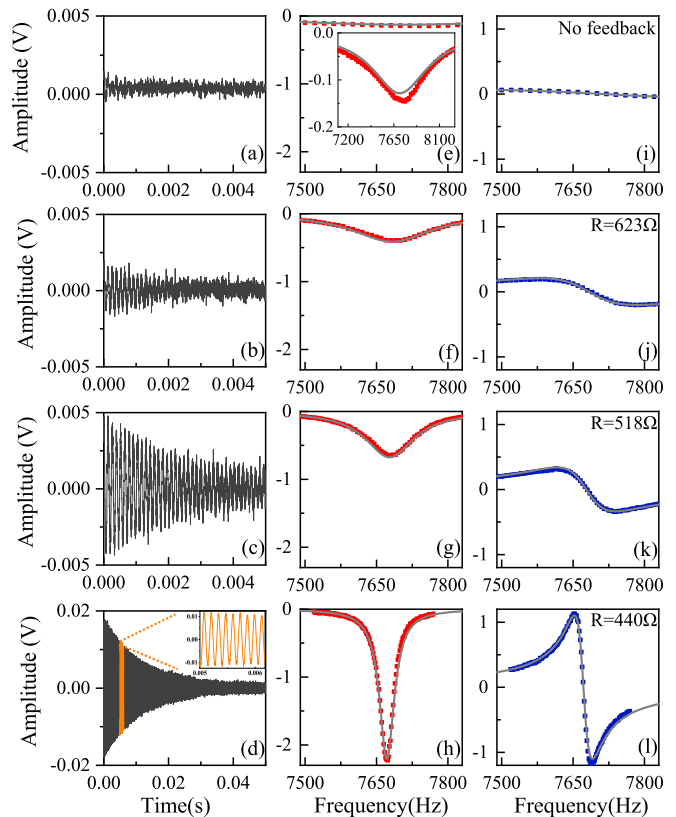


FIG. 3. From (a) to (e) are the output signals of the BPD after turning off the driving magnetic field B_x . The inset in the (d) is a zoomed-in view of the orange area. From (e) to (h) and (i) to (l) are the out of phase and in phase output signals of the lock-in amplifier, respectively. The inset in the (e) shows a larger frequency range. The scatters are experimental results and the gray solid curves are theoretical results. From top to bottom, the feedback resistance decreases with the values labeled in the figure.

a feedback resistor and the y -axis feedback coil, which generates the feedback magnetic field $B_y = -\Gamma_{\text{FB}}P_x/\gamma$ with Γ_{FB} being the feedback factor. No noise processing of the signal is necessary because the signal-to-noise ratio in our experiments is large enough. In this case the feedback magnetic field B_y carries the information of the spin polarization component P_x , which will result in \mathcal{PT} -symmetric feedback.

When the feedback magnetic field B_y is small compared with the static magnetic field B_0 , its effect on P_z can be ignored, and P_z remains equilibrium polarization P_0 . Starting from the Bloch equations, we obtain the simplified equations containing only two orthogonal components (P_x, P_y) as

$$\begin{cases} \dot{P}_x = \left(\Gamma_{\text{FB}}P_0 - \frac{1}{T_2}\right)P_x + \omega_0P_y, \\ \dot{P}_y = -\omega_0P_x - \frac{1}{T_2}P_y, \end{cases} \quad (3)$$

where T_2 is the transverse relaxation time. The dynamics

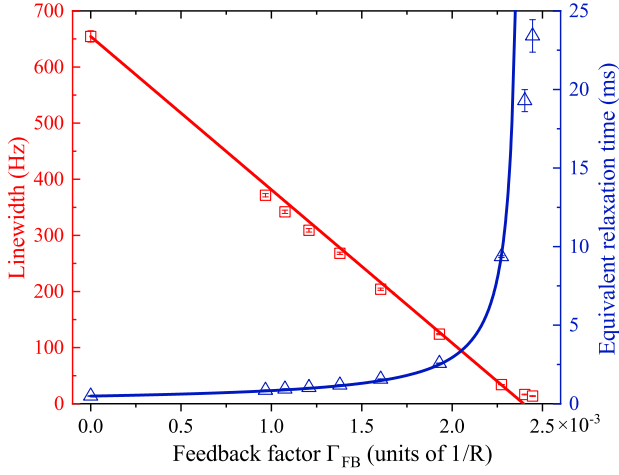


FIG. 4. Dependence of linewidth and equivalent relaxation time on the feedback factor. The scatters are experimental results and the red and blue solid line is the theoretical result.

can be effectively described by

$$H_{\text{eff}} = \begin{pmatrix} i\frac{P_0}{2}\Gamma_{\text{FB}} & i\omega_0 \\ -i\omega_0 & -i\frac{P_0}{2}\Gamma_{\text{FB}} \end{pmatrix} + i \left(\frac{P_0}{2}\Gamma_{\text{FB}} - \frac{1}{T_2} \right) \mathbf{I}, \quad (4)$$

which is equivalent to Eq. (2) with $\kappa = 1/T_2$ and $\Gamma = \Gamma_{\text{FB}}P_0$. Therefore, the collective spin oscillator constitutes a \mathcal{PT} -symmetric system.

Next we focus on the \mathcal{PT} -symmetric phase ($\Gamma_{\text{FB}}P_0 < 2\omega_0$) and show the ability of linewidth narrowing. The imaginary part of the eigenvalues is $\Gamma_{\text{FB}}P_0/2 - 1/T_2$, thus the linewidth $\Delta\omega_{\text{FWHM}}$ is

$$\Delta\omega_{\text{FWHM}} = \frac{2}{T_2} - \Gamma_{\text{FB}}P_0. \quad (5)$$

As the feedback factor Γ_{FB} increases, the system dissipation keeps reducing, and the resonance linewidth keeps narrowing. In our experiment, the feedback factor is inversely proportional to the feedback resistance ($\Gamma_{\text{FB}} \propto 1/R$). Therefore, our scheme enables flexible adjusting of the linewidth by changing the feedback factor Γ_{FB} through the resistance R .

In order to measure the resonance linewidth, we apply a weak driving magnetic field $B_x = B_1 \cos(\omega t)$ along x axis, which corresponds to an additional term $\gamma B_1 \cos(\omega t)$ in the equation of P_y in Eq. (3). Then the system undergoes forced oscillation, and we can use instantaneous drive with sudden tuning off to obtain the system evolution dynamics in the time domain, or use continuous drive with scanning frequency ω to obtain the system response in the frequency domain. In Fig. 3, the time domain signals (first column), frequency domain absorption signals (second column) and dispersion signals (third column) are plotted. From top to bottom, as the feedback resistance R decreases (corresponding to the increase of the feedback factor Γ_{FB}), it

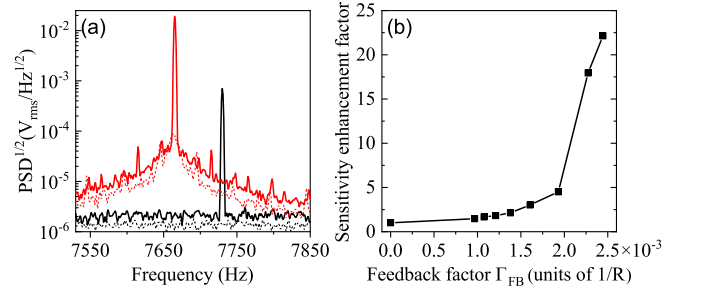


FIG. 5. (a) Square root of power spectral density ($\text{PSD}^{1/2}$) for feedback resistance $R = 409 \Omega$ (red curves) and without feedback (black curves). The solid (dashed) curves are the results in the presence (absence) of driving magnetic field B_x . (b) Sensitivity enhancement factor of the M_x magnetometer as a function of the feedback factor.

shows clearly that the oscillation lasts longer, and the absorption linewidth becomes narrower, and the dispersion slope becomes sharper. The experimental results are in good agreement with the theoretical predictions, where the feedback delay has been taken into account (see Supplemental Material [102]).

The dependencies of linewidth and equivalent relaxation time on the feedback factor are plotted in Fig. 4. In the experiment, we have observed the reduction of the linewidth from 654 to 13.6 Hz, which is 48 times narrower. The equivalent relaxation time increases from 0.486 to 23.4 ms, which significantly extends the coherence time of the system. Further improvement is limited by the stability of the present experimental system, as it becomes more sensitive to the parameter variations when the linewidth is very narrow.

The \mathcal{PT} -symmetric feedback induced linewidth narrowing method holds great potential for high-precision measurements. Our experimental system can be directly used to improve the measurement sensitivity of magnetic field, with the apparatus similar to the M_x magnetometer [103, 104]. When the driving magnetic field is on resonance with the Larmor frequency $\omega_0 = \gamma B_0$, the spin polarization P_x reaches its maximum value. Thus the magnitude of the magnetic field B_0 can be obtained by scanning the frequency of the driving magnetic field. The measurement sensitivity of this M_x magnetometer is [102–104]

$$\delta B = k_F \frac{\Delta\omega_{\text{FWHM}}}{\gamma} \frac{1}{S/N}, \quad (6)$$

where $k_F = \frac{1}{2\sqrt{2}}$. To obtain the signal-to-noise ratio S/N , we measure the square root of the power spectral density ($\text{PSD}^{1/2}$) by feeding the output of time domain signals into the fast Fourier transformation (FFT) spectrum analyzer (SR760). As compared in Fig. 5(a), the signal with feedback is significantly larger compared to that without feedback. As the background noise also increases, the signal-to-noise ratio stays almost unchanged.

The shift of resonance frequency originates from the relaxation and the feedback with delay (see Supplemental Material [102]), which does not affect the measurement sensitivity for small changes of magnetic field. According to Eq. (6), we can obtain the dependence of sensitivity on the feedback factor, as plotted in Fig. 5(b). The sensitivity of the M_x magnetometer is enhanced up to 22 times, with the linewidth narrowing playing a significant role in this enhancement. Compared with the 48-fold reduction of the linewidth, this 22-times enhancement of the measurement sensitivity indicates some additional noise in the feedback process, which may be overcome by further stabilizing the feedback loop.

In summary, we propose a \mathcal{PT} -symmetric feedback method in a general dissipative resonance system. By constructing a quadrature measurement-feedback loop in which one quadrature component is measured with feedback, a purely dissipative resonance system can be transformed into a \mathcal{PT} -symmetric system, with tunable \mathcal{PT} -symmetric phase and \mathcal{PT} -symmetry-broken phase. Such a \mathcal{PT} -symmetric system contains only a single resonance mode, without the requirement of two or more modes, as the feedback breaks the symmetry between the quadratures, and thus the two quadratures of a single resonance mode behave like two different modes. The method finds important applications in linewidth narrowing and enhancement of measurement sensitivity. We demonstrate the proposal in a thermal atomic ensemble and observe a 48-fold narrowing of the magnetic resonance linewidth. By applying the method in the M_x magnetometer, we realize a 22-times enhancement of the magnetic field measurement sensitivity. It can also be directly applied to other precision measurement experiments limited by linewidth such as atomic gyroscope. Our study provides a new perspective on using feedback to construct \mathcal{PT} -symmetric systems, which form an excellent platform for studying non-Hermitian physics, with broad applications in high-precision measurement and sensing.

This work is supported by the Key-Area Research and Development Program of Guangdong Province (Grants No. 2019B030330001), the National Natural Science Foundation of China (NSFC) (Grants No. 12275145, No. 92050110, No. 91736106, No. 11674390, and No. 91836302), and the National Key R&D Program of China (Grants No. 2018YFA0306504).

* ycliu@tsinghua.edu.cn

- [1] I. K. Komninos, T. W. Kornack, J. C. Allred, and M. V. Romalis, *Nature (London)* **422**, 596 (2003).
- [2] D. Budker and M. Romalis, *Nat. Phys.* **3**, 227 (2007).
- [3] T. W. Kornack, R. K. Ghosh, and M. V. Romalis, *Phys. Rev. Lett.* **95**, 230801 (2005).
- [4] M. Siefert, S. Lehmkuhl, A. Liebisch, B. Blümich, and S. Appelt, *Nat. Phys.* **13**, 568 (2017).
- [5] M. Jiang, H. Su, A. Garcon, X. Peng, and D. Budker, *Nat. Phys.* **17**, 1402 (2021).
- [6] S. Afach, B. C. Buchler, D. Budker, C. Dailey, A. Derevianko, V. Dumont, N. L. Figueroa, I. Gerhardt, Z. D. Grujić, H. Guo, *et al.*, *Nat. Phys.* **17**, 1396 (2021).
- [7] H. Su, Y. Wang, M. Jiang, W. Ji, P. Fadeev, D. Hu, X. Peng, and D. Budker, *Sci. Adv.* **7**, eabi9535 (2021).
- [8] Z. Wu, *Rev. Mod. Phys.* **93**, 035006 (2021).
- [9] M. V. Balabas, T. Karaulanov, M. P. Ledbetter, and D. Budker, *Phys. Rev. Lett.* **105**, 070801 (2010).
- [10] K. F. Zhao, M. Schaden, and Z. Wu, *Phys. Rev. A* **78**, 034901 (2008).
- [11] W. Happer and H. Tang, *Phys. Rev. Lett.* **31**, 273 (1973).
- [12] J. C. Allred, R. N. Lyman, T. W. Kornack, and M. V. Romalis, *Phys. Rev. Lett.* **89**, 130801 (2002).
- [13] D. Budker, W. Gawlik, D. F. Kimball, S. M. Rochester, V. V. Yashchuk, and A. Weis, *Rev. Mod. Phys.* **74**, 1153 (2002).
- [14] M. O. Scully and M. Fleischhauer, *Phys. Rev. Lett.* **69**, 1360 (1992).
- [15] C. M. Bender and S. Boettcher, *Phys. Rev. Lett.* **80**, 5243 (1998).
- [16] L. Feng, R. El-Ganainy, and L. Ge, *Nat. Photonics* **11**, 752 (2017).
- [17] R. El-Ganainy, K. G. Makris, M. Khajavikhan, Z. H. Musslimani, S. Rotter, and D. N. Christodoulides, *Nat. Phys.* **14**, 11 (2018).
- [18] Ş. K. Özdemir, S. Rotter, F. Nori, and L. Yang, *Nat. Mater.* **18**, 783 (2019).
- [19] K. G. Makris, R. El-Ganainy, D. N. Christodoulides, and Z. H. Musslimani, *Phys. Rev. Lett.* **100**, 103904 (2008).
- [20] A. Guo, G. J. Salamo, D. Duchesne, R. Morandotti, M. Volatier-Ravat, V. Aimez, G. A. Siviloglou, and D. N. Christodoulides, *Phys. Rev. Lett.* **103**, 093902 (2009).
- [21] C. E. Rüter, K. G. Makris, R. El-Ganainy, D. N. Christodoulides, M. Segev, and D. Kip, *Nat. Phys.* **6**, 192 (2010).
- [22] A. Regensburger, C. Bersch, M.-A. Miri, G. Onishchukov, D. N. Christodoulides, and U. Peschel, *Nature (London)* **488**, 167 (2012).
- [23] L. Chang, X. Jiang, S. Hua, C. Yang, J. Wen, L. Jiang, G. Li, G. Wang, and M. Xiao, *Nat. Photonics* **8**, 524 (2014).
- [24] B. Peng, Ş. K. Özdemir, F. Lei, F. Monifi, M. Gianfreda, G. L. Long, S. Fan, F. Nori, C. M. Bender, and L. Yang, *Nat. Phys.* **10**, 394 (2014).
- [25] L. Feng, Z. J. Wong, R.-M. Ma, Y. Wang, and X. Zhang, *Science* **346**, 972 (2014).
- [26] C. Hang, G. Huang, and V. V. Konotop, *Phys. Rev. Lett.* **110**, 083604 (2013).
- [27] Z. Zhang, Y. Zhang, J. Sheng, L. Yang, M.-A. Miri, D. N. Christodoulides, B. He, Y. Zhang, and M. Xiao, *Phys. Rev. Lett.* **117**, 123601 (2016).
- [28] J. Li, A. K. Harter, J. Liu, L. de Melo, Y. N. Joglekar, and L. Luo, *Nat. Commun.* **10**, 855 (2019).
- [29] L. Ding, K. Shi, Q. Zhang, D. Shen, X. Zhang, and W. Zhang, *Phys. Rev. Lett.* **126**, 083604 (2021).
- [30] J. Schindler, A. Li, M. C. Zheng, F. M. Ellis, and T. Kottos, *Phys. Rev. A* **84**, 040101(R) (2011).
- [31] Y. Sun, W. Tan, H.-q. Li, J. Li, and H. Chen, *Phys. Rev. Lett.* **112**, 143903 (2014).

- [32] X. Yang, J. Li, Y. Ding, M. Xu, X.-F. Zhu, and J. Zhu, *Phys. Rev. Lett.* **128**, 065701 (2022).
- [33] Y. Wu, W. Liu, J. Geng, X. Song, X. Ye, C.-K. Duan, X. Rong, and J. Du, *Science* **364**, 878 (2019).
- [34] H. Jing, S. K. Özdemir, X.-Y. Lü, J. Zhang, L. Yang, and F. Nori, *Phys. Rev. Lett.* **113**, 053604 (2014).
- [35] X.-Y. Lü, H. Jing, J.-Y. Ma, and Y. Wu, *Phys. Rev. Lett.* **114**, 253601 (2015).
- [36] X.-W. Xu, Y.-x. Liu, C.-P. Sun, and Y. Li, *Phys. Rev. A* **92**, 013852 (2015).
- [37] D. W. Schönleber, A. Eisfeld, and R. El-Ganainy, *New J. Phys.* **18**, 045014 (2016).
- [38] J. Zhang, B. Peng, Ş. K. Özdemir, K. Pichler, D. O. Krimer, G. Zhao, F. Nori, Y.-x. Liu, S. Rotter, and L. Yang, *Nat. Photonics* **12**, 479 (2018).
- [39] X. Zhu, H. Ramezani, C. Shi, J. Zhu, and X. Zhang, *Phys. Rev. X* **4**, 031042 (2014).
- [40] R. Fleury, D. Sounas, and A. Alù, *Nat. Commun.* **6**, 5905 (2015).
- [41] S. Bittner, B. Dietz, U. Günther, H. L. Harney, M. Miski-Oglu, A. Richter, and F. Schäfer, *Phys. Rev. Lett.* **108**, 024101 (2012).
- [42] H. Hodaie, A. U. Hassan, S. Wittek, H. Garcia-Gracia, R. El-Ganainy, D. N. Christodoulides, and M. Khajavikhan, *Nature (London)* **548**, 187 (2017).
- [43] W. Chen, Ş. Kaya Özdemir, G. Zhao, J. Wiersig, and L. Yang, *Nature (London)* **548**, 192 (2017).
- [44] Y.-H. Lai, Y.-K. Lu, M.-G. Suh, Z. Yuan, and K. Vahala, *Nature (London)* **576**, 65 (2019).
- [45] Z. Xiao, H. Li, T. Kottos, and A. Alù, *Phys. Rev. Lett.* **123**, 213901 (2019).
- [46] R. Kononchuk, J. Cai, F. Ellis, R. Thevamaran, and T. Kottos, *Nature (London)* **607**, 697 (2022).
- [47] J. Bechhoefer, *Rev. Mod. Phys.* **77**, 783 (2005).
- [48] H. M. Wiseman, *Phys. Rev. A* **49**, 2133 (1994).
- [49] A. Hopkins, K. Jacobs, S. Habib, and K. Schwab, *Phys. Rev. B* **68**, 235328 (2003).
- [50] D. Kleckner and D. Bouwmeester, *Nature (London)* **444**, 75 (2006).
- [51] R. Hamerly and H. Mabuchi, *Phys. Rev. Lett.* **109**, 173602 (2012).
- [52] D. J. Wilson, V. Sudhir, N. Piro, R. Schilling, A. Ghadimi, and T. J. Kippenberg, *Nature (London)* **524**, 325 (2015).
- [53] M. Rossi, N. Kralj, S. Zippilli, R. Natali, A. Borrielli, G. Pandraud, E. Serra, G. Di Giuseppe, and D. Vitali, *Phys. Rev. Lett.* **119**, 123603 (2017).
- [54] J. Guo, R. Norte, and S. Gröblacher, *Phys. Rev. Lett.* **123**, 223602 (2019).
- [55] F. Tebbenjohanns, M. Frimmer, A. Militaru, V. Jain, and L. Novotny, *Phys. Rev. Lett.* **122**, 223601 (2019).
- [56] C. Sommer and C. Genes, *Phys. Rev. Lett.* **123**, 203605 (2019).
- [57] F. van der Laan, F. Tebbenjohanns, R. Reimann, J. Vijayan, L. Novotny, and M. Frimmer, *Phys. Rev. Lett.* **127**, 123605 (2021).
- [58] C. Whittle, E. D. Hall, S. Dwyer, N. Mavalvala, V. Sudhir, R. Abbott, A. Ananyeva, C. Austin, L. Barsotti, J. Betzwieser, et al., *Science* **372**, 1333 (2021).
- [59] G.-L. Schmid, C. T. Ngai, M. Ernzer, M. B. Aguilera, T. M. Karg, and P. Treutlein, *Phys. Rev. X* **12**, 011020 (2022).
- [60] M. Koch, C. Sames, A. Kubanek, M. Apel, M. Balbach, A. Ourjoumtsev, P. W. H. Pinkse, and G. Rempe, *Phys. Rev. Lett.* **105**, 173003 (2010).
- [61] N. Behbood, G. Colangelo, F. Martin Ciurana, M. Napolitano, R. J. Sewell, and M. W. Mitchell, *Phys. Rev. Lett.* **111**, 103601 (2013).
- [62] M. R. Hush, S. S. Szigeti, A. R. R. Carvalho, and J. J. Hope, *New J. Phys.* **15**, 113060 (2013).
- [63] D. A. Ivanov and T. Y. Ivanova, *J. Phys. B: At. Mol. Opt. Phys.* **47**, 135303 (2014).
- [64] M. Schemmer, A. Johnson, R. Photopoulos, and I. Bouchoule, *Phys. Rev. A* **95**, 043641 (2017).
- [65] W. Kopylov, C. Emary, E. Schöll, and T. Brandes, *New J. Phys.* **17**, 013040 (2015).
- [66] H. M. Hurst and I. B. Spielman, *Phys. Rev. A* **99**, 053612 (2019).
- [67] H. M. Hurst, S. Guo, and I. B. Spielman, *Phys. Rev. Res.* **2**, 043325 (2020).
- [68] D. A. Ivanov, T. Y. Ivanova, S. F. Caballero-Benitez, and I. B. Mekhov, *Phys. Rev. Lett.* **124**, 010603 (2020).
- [69] G. Buonaiuto, F. Carollo, B. Olmos, and I. Lesanovsky, *Phys. Rev. Lett.* **127**, 133601 (2021).
- [70] M. H. Muñoz-Arias, I. H. Deutsch, P. S. Jessen, and P. M. Poggi, *Phys. Rev. A* **102**, 022610 (2020).
- [71] J. Geremia, *Phys. Rev. Lett.* **97**, 073601 (2006).
- [72] M. Yanagisawa, *Phys. Rev. Lett.* **97**, 190201 (2006).
- [73] A. Negretti, U. V. Poulsen, and K. Mølmer, *Phys. Rev. Lett.* **99**, 223601 (2007).
- [74] C. Sayrin, I. Dotsenko, X. Zhou, B. Peaudecerf, T. Rybarczyk, S. Gleyzes, P. Rouchon, M. Mirrahimi, H. Amini, M. Brune, J.-M. Raimond, and S. Haroche, *Nature (London)* **477**, 73 (2011).
- [75] X. Zhou, I. Dotsenko, B. Peaudecerf, T. Rybarczyk, C. Sayrin, S. Gleyzes, J. M. Raimond, M. Brune, and S. Haroche, *Phys. Rev. Lett.* **108**, 243602 (2012).
- [76] M. Gajdacz, A. J. Hilliard, M. A. Kristensen, P. L. Pedersen, C. Klempt, J. J. Arlt, and J. F. Sherson, *Phys. Rev. Lett.* **117**, 073604 (2016).
- [77] J. Lammers, H. Weimer, and K. Hammerer, *Phys. Rev. A* **94**, 052120 (2016).
- [78] L.-N. Wu and A. Eckardt, *Phys. Rev. Res.* **4**, L022045 (2022).
- [79] N. V. Morrow, S. K. Dutta, and G. Raithel, *Phys. Rev. Lett.* **88**, 093003 (2002).
- [80] D. A. Steck, K. Jacobs, H. Mabuchi, T. Bhattacharya, and S. Habib, *Phys. Rev. Lett.* **92**, 223004 (2004).
- [81] R. Vijay, C. Macklin, D. H. Slichter, S. J. Weber, K. W. Murch, R. Naik, A. N. Korotkov, and I. Siddiqi, *Nature (London)* **490**, 77 (2012).
- [82] A. Carmele, J. Kabuss, F. Schulze, S. Reitzenstein, and A. Knorr, *Phys. Rev. Lett.* **110**, 013601 (2013).
- [83] T. Vanderbruggen, R. Kohlhaas, A. Bertoldi, S. Bernon, A. Aspect, A. Landragin, and P. Bouyer, *Phys. Rev. Lett.* **110**, 210503 (2013).
- [84] J. Kohler, N. Spethmann, S. Schreppler, and D. M. Stamper-Kurn, *Phys. Rev. Lett.* **118**, 063604 (2017).
- [85] K. Kroeger, N. Dogra, R. Rosa-Medina, M. Paluch, F. Ferri, T. Donner, and T. Esslinger, *New J. Phys.* **22**, 033020 (2020).
- [86] J. T. Young, A. V. Gorshkov, and I. B. Spielman, *Phys. Rev. Res.* **3**, 043075 (2021).
- [87] M. Jiang, H. Su, Z. Wu, X. Peng, and D. Budker, *Sci. Adv.* **7**, eabe0719 (2021).
- [88] S. Lloyd and J.-J. E. Slotine, *Phys. Rev. A* **62**, 012307

- (2000).
- [89] Z.-P. Liu, H. Wang, J. Zhang, Y.-x. Liu, R.-B. Wu, C.-W. Li, and F. Nori, *Phys. Rev. A* **88**, 063851 (2013).
- [90] M. H. Muñoz-Arias, P. M. Poggi, P. S. Jessen, and I. H. Deutsch, *Phys. Rev. Lett.* **124**, 110503 (2020).
- [91] M. T. Cuairan, J. Gieseler, N. Meyer, and R. Quidant, *Phys. Rev. Lett.* **128**, 213601 (2022).
- [92] N. Yamamoto, *Phys. Rev. Appl.* **5**, 044012 (2016).
- [93] R. Shimazu and N. Yamamoto, *Phys. Rev. Appl.* **15**, 044006 (2021).
- [94] L. K. Thomsen, S. Mancini, and H. M. Wiseman, *Phys. Rev. A* **65**, 061801(R) (2002).
- [95] R. Inoue, S.-I.-R. Tanaka, R. Namiki, T. Sagawa, and Y. Takahashi, *Phys. Rev. Lett.* **110**, 163602 (2013).
- [96] A. C. J. Wade, J. F. Sherson, and K. Mølmer, *Phys. Rev. Lett.* **115**, 060401 (2015).
- [97] K. C. Cox, G. P. Greve, J. M. Weiner, and J. K. Thompson, *Phys. Rev. Lett.* **116**, 093602 (2016).
- [98] J. Wang, H. M. Wiseman, and G. J. Milburn, *Phys. Rev. A* **71**, 042309 (2005).
- [99] A. R. R. Carvalho, A. J. S. Reid, and J. J. Hope, *Phys. Rev. A* **78**, 012334 (2008).
- [100] D. Ristè, M. Dukalski, C. A. Watson, G. de Lange, M. J. Tiggelman, Y. M. Blanter, K. W. Lehnert, R. N. Schouten, and L. DiCarlo, *Nature (London)* **502**, 350 (2013).
- [101] V. Sudhir, D. J. Wilson, R. Schilling, H. Schütz, S. A. Fedorov, A. H. Ghadimi, A. Nunnenkamp, and T. J. Kippenberg, *Phys. Rev. X* **7**, 011001 (2017).
- [102] See Supplemental Material for the theoretical model of feedback with delay, the PT-symmetric feedback in the optical cavity, and experimental details..
- [103] S. Groeger, G. Bison, J.-L. Schenker, R. Wynands, and A. Weis, *Eur. Phys. J. D* **38**, 239 (2006).
- [104] D. Budker and D. F. J. Kimball, eds., *Optical Magnetometry* (Cambridge University Press, 2013).

Supplemental Material for “ \mathcal{PT} -symmetric feedback induced linewidth narrowing”

Yuanjiang Tang¹, Chao Liang¹, Xin Wen¹, Weipeng Li¹, An-Ning Xu¹ and Yong-Chun Liu^{1,2*}

¹*State Key Laboratory of Low-Dimensional Quantum Physics,*

Department of Physics, Tsinghua University, Beijing 100084, China and

²*Frontier Science Center for Quantum Information, Beijing 100084, China*

(Dated: May 18, 2023)

CONTENTS

I. Theoretical model of feedback with delay	1
A. Theoretical model of feedback with delay and noise	3
II. \mathcal{PT} -symmetric feedback in the optical cavity	5
III. Experimental details	6
A. Derivation of the feedback factor	6
B. Experimental parameters	6
C. Energy level diagram and laser frequencies	7
D. Principle of measuring the spin polarizability P_x	7
E. Sequence diagram of the drives for two linewidth measurement schemes	8
F. Discussion of measuring magnetic field and sensitivity	8
1. Method of measuring the magnetic field in the z -axis	8
2. Derivation of the sensitivity formula	9
3. Experimental measurement procedures for signal-to-noise ratio and sensitivity	10

I. THEORETICAL MODEL OF FEEDBACK WITH DELAY

In the \mathcal{PT} -symmetric feedback method as described in the main text, the x -component of the spin polarization P_x is measured, and then fed back to the y -axis magnetic field coil. In general, there is typically a delay time τ between the feedback and the measurement processes. Because of the delay, the magnetic field generated by the feedback at time t is proportional to the measured spin polarization at $t - \tau$, which can be written as

$$B_y(t) = -\frac{\Gamma_{\text{FB}}}{\gamma} P_x(t - \tau), \quad (\text{S1})$$

where Γ_{FB} is the feedback factor and γ is the gyromagnetic ratio of the atom. When the delay time τ is much smaller than the characteristic time of the system mentioned below (i.e., the relaxation time T_2 and the oscillation period $2\pi/\omega_0$), we can use Taylor expansion and retain the first-order term of τ , yielding

$$P_x(t - \tau) = P_x(t) - \tau \dot{P}_x(t). \quad (\text{S2})$$

Now all the physical quantities are at time t , so the time variable t is omitted below.

The total magnetic field vector is

$$\mathbf{B} = (B_x, B_y, B_z) = \left(B_1 \cos(\omega t), -\frac{\Gamma_{\text{FB}}}{\gamma} (P_x - \tau \dot{P}_x), B_0 \right), \quad (\text{S3})$$

where B_x is the weak driving magnetic field applied to measure the system properties, B_y is the feedback magnetic field, and B_z is the static bias magnetic field. The dynamic of the spin polarization $\mathbf{P} = (P_x, P_y, P_z)$ can be described

* ycliu@tsinghua.edu.cn

by the Bloch equation

$$\begin{cases} \dot{P}_x = \gamma (P_y B_z - P_z B_y) - \frac{P_x}{T_2}, \\ \dot{P}_y = \gamma (-P_x B_z + P_z B_x) - \frac{P_y}{T_2}, \\ \dot{P}_z = \gamma (P_x B_y - P_y B_x) - \frac{P_z}{T_1} + R_{\text{op}}, \end{cases} \quad (\text{S4})$$

where T_1 is the longitudinal relaxation time, T_2 is the transverse relaxation time, and R_{op} is the rate of optical pumping. Putting the expression of total magnetic field \mathbf{B} into Eq.(S4) gives

$$\dot{P}_x = \omega_0 P_y + \Gamma_{\text{FB}} P_z \left(P_x - \tau \dot{P}_x \right) - \frac{P_x}{T_2}, \quad (\text{S5})$$

$$\dot{P}_y = -\omega_0 P_x + \omega_1 P_z \cos(\omega t) - \frac{P_y}{T_2}, \quad (\text{S6})$$

$$\dot{P}_z = -\Gamma_{\text{FB}} P_x \left(P_x - \tau \dot{P}_x \right) - P_y \omega_1 \cos(\omega t) - \frac{P_z}{T_1} + R_{\text{op}}, \quad (\text{S7})$$

where $\omega_0 = \gamma B_0$, $\omega_1 = \gamma B_1$.

In Eq.(S7), when the feedback factor Γ_{FB} is small compared with the optical pumping rate R_{op} , the nonlinear term $-\Gamma_{\text{FB}} P_x (P_x - \tau \dot{P}_x)$ can be ignored. B_1 is also small as it is a weak magnetic field applied to measure the system properties, so the driving term $-P_y \omega_1 \cos(\omega t)$ can be neglected. Then P_z reaches the steady state, corresponding to the equilibrium polarization $P_z = P_0 = R_{\text{op}} T_1$, which keeps a constant in the experiment.

From Eq.(S5) we obtain

$$\dot{P}_x = \frac{\Gamma_{\text{FB}} P_0 - \frac{1}{T_2}}{1 + \Gamma_{\text{FB}} P_0 \tau} P_x + \frac{\omega_0}{1 + \Gamma_{\text{FB}} P_0 \tau} P_y. \quad (\text{S8})$$

From Eq.(S8) we obtain the derivative as

$$\ddot{P}_x = \frac{\Gamma_{\text{FB}} P_0 - \frac{1}{T_2}}{1 + \Gamma_{\text{FB}} P_0 \tau} \dot{P}_x + \frac{\omega_0}{1 + \Gamma_{\text{FB}} P_0 \tau} \dot{P}_y. \quad (\text{S9})$$

Inserting \dot{P}_y given by Eq.(S6) into Eq.(S9), we obtain

$$\ddot{P}_x = \frac{\Gamma_{\text{FB}} P_0 - \frac{1}{T_2}}{1 + \Gamma_{\text{FB}} P_0 \tau} \dot{P}_x - \frac{\omega_0^2}{1 + \Gamma_{\text{FB}} P_0 \tau} P_x - \frac{\omega_0}{(1 + \Gamma_{\text{FB}} P_0 \tau) T_2} P_y + \frac{\omega_0 \omega_1 P_0}{1 + \Gamma_{\text{FB}} P_0 \tau} \cos \omega t. \quad (\text{S10})$$

From Eq.(S8), we obtain the expression of P_y as

$$P_y = \frac{1}{\omega_0} \left[(1 + \Gamma_{\text{FB}} P_0 \tau) \dot{P}_x - \Gamma_{\text{FB}} P_x P_0 + \frac{P_x}{T_2} \right]. \quad (\text{S11})$$

Putting it into Eq.(S10), finally we obtain

$$\ddot{P}_x + \left(\frac{1}{T_2} - \frac{\Gamma_{\text{FB}} P_0 - \frac{1}{T_2}}{1 + \Gamma_{\text{FB}} P_0 \tau} \right) \dot{P}_x + \left[\frac{\omega_0^2}{1 + \Gamma_{\text{FB}} P_0 \tau} - \frac{\Gamma_{\text{FB}} P_0 - \frac{1}{T_2}}{(1 + \Gamma_{\text{FB}} P_0 \tau) T_2} \right] P_x = \frac{\omega_0 \omega_1 P_0}{1 + \Gamma_{\text{FB}} P_0 \tau} \cos \omega t. \quad (\text{S12})$$

This describes a typical forced harmonic oscillation with a driving force, which can be abbreviated as

$$\ddot{P}_x + \Gamma_{\text{eff}} \dot{P}_x + \omega_{\text{eff}}^2 P_x = \frac{\omega_0 \omega_1 P_0}{1 + \Gamma_{\text{FB}} P_0 \tau} \cos \omega t, \quad (\text{S13})$$

where

$$\Gamma_{\text{eff}} = \frac{1}{T_2} - \frac{\Gamma_{\text{FB}} P_0 - \frac{1}{T_2}}{1 + \Gamma_{\text{FB}} P_0 \tau}, \quad (\text{S14})$$

$$\omega_{\text{eff}} = \sqrt{\frac{\omega_0^2}{1 + \Gamma_{\text{FB}} P_0 \tau} - \frac{\Gamma_{\text{FB}} P_0 - \frac{1}{T_2}}{(1 + \Gamma_{\text{FB}} P_0 \tau) T_2}}. \quad (\text{S15})$$

In order to calculate P_x , we can set $P_x = \text{Re}[\tilde{P}_x e^{i\omega t}]$ and put it into Eq.(S13), then \tilde{P}_x satisfies the equation

$$(-\omega^2 + i\Gamma_{\text{eff}}\omega + \omega_{\text{eff}}^2)\tilde{P}_x e^{i\omega t} = \frac{\omega_0\omega_1 P_0}{1 + \Gamma_{\text{FB}}P_0\tau} e^{i\omega t} \quad (\text{S16})$$

The solution of Eq.(S16) is

$$\tilde{P}_x = \frac{\frac{\omega_0\omega_1 P_0}{1 + \Gamma_{\text{FB}}P_0\tau}}{\omega_{\text{eff}}^2 - \omega^2 + i\Gamma_{\text{eff}}\omega} = \frac{\frac{\omega_0\omega_1 P_0}{1 + \Gamma_{\text{FB}}P_0\tau} (\omega_{\text{eff}}^2 - \omega^2)}{(\omega_{\text{eff}}^2 - \omega^2)^2 + \Gamma_{\text{eff}}^2\omega^2} - i \frac{\frac{\omega_0\omega_1 P_0}{1 + \Gamma_{\text{FB}}P_0\tau} \Gamma_{\text{eff}}\omega}{(\omega_{\text{eff}}^2 - \omega^2)^2 + \Gamma_{\text{eff}}^2\omega^2}. \quad (\text{S17})$$

So we obtain

$$P_x = \text{Re} [\tilde{P}_x e^{i\omega t}] = \frac{\frac{\omega_0\omega_1 P_0}{1 + \Gamma_{\text{FB}}P_0\tau} (\omega_{\text{eff}}^2 - \omega^2)}{(\omega_{\text{eff}}^2 - \omega^2)^2 + \Gamma_{\text{eff}}^2\omega^2} \cos(\omega t) + \frac{\frac{\omega_0\omega_1 P_0}{1 + \Gamma_{\text{FB}}P_0\tau} \Gamma_{\text{eff}}\omega}{(\omega_{\text{eff}}^2 - \omega^2)^2 + \Gamma_{\text{eff}}^2\omega^2} \sin(\omega t). \quad (\text{S18})$$

When near resonance ($\omega \approx \omega_{\text{eff}}$), the above equation can be simplified as

$$P_x \simeq \frac{\frac{\omega_0\omega_1 P_0}{2\omega_{\text{eff}}(1 + \Gamma_{\text{FB}}P_0\tau)} (\omega_{\text{eff}} - \omega)}{(\omega_{\text{eff}} - \omega)^2 + \frac{\Gamma_{\text{eff}}^2}{4}} \cos(\omega t) + \frac{\frac{\omega_0\omega_1 P_0}{4\omega_{\text{eff}}(1 + \Gamma_{\text{FB}}P_0\tau)} \Gamma_{\text{eff}}}{(\omega_{\text{eff}} - \omega)^2 + \frac{\Gamma_{\text{eff}}^2}{4}} \sin(\omega t). \quad (\text{S19})$$

The spin polarization P_x contains two orthogonal components, $\cos(\omega t)$ term and $\sin(\omega t)$ term, which correspond to the dispersion and absorption properties, respectively. In Fig. 3 of the main text, the curves are fitted with the two components in Eq.(S19).

When the feedback delay is relatively small with $\Gamma_{\text{FB}}P_0\tau \ll 1$, from Eq.(S14) and Eq.(S15), we can obtain

$$\Gamma_{\text{eff}} \simeq \frac{2}{T_2} - \Gamma_{\text{FB}}P_0, \quad (\text{S20})$$

$$\omega_{\text{eff}} \simeq \sqrt{\omega_0^2 - \Gamma_{\text{FB}}P_0\tau\omega_0^2 - \frac{1}{T_2^2}}. \quad (\text{S21})$$

Therefore, the impact of delay time τ on the linewidth is negligible, while its impact on the resonance frequency is relatively large. In Fig. 5(a) of the main text, the resonance shift is determined by Eq.(S21).

A. Theoretical model of feedback with delay and noise

In the original feedback model, we assumed that the total noise during the measurement is N , so the measured spin polarization P_x should be added with this noise, and then fed back to the y -axis magnetic field B_y , so

$$B_y(t) = -\frac{\Gamma_{\text{FB}}}{\gamma} (P_x(t - \tau) + N). \quad (\text{S22})$$

Considering the noise, the total magnetic field feedback is

$$\mathbf{B} = (B_x, B_y, B_z) = \left(B_1 \cos(\omega t), -\frac{\Gamma_{\text{FB}}}{\gamma} (P_x - \tau\dot{P}_x + N), B_0 \right), \quad (\text{S23})$$

Putting the expression of total magnetic field \mathbf{B} into Eq.(S4) gives

$$\dot{P}_x = \omega_0 P_y + \Gamma_{\text{FB}} P_z \left(P_x - \tau\dot{P}_x + N \right) - \frac{P_x}{T_2}, \quad (\text{S24})$$

$$\dot{P}_y = -\omega_0 P_x + \omega_1 P_z \cos(\omega t) - \frac{P_y}{T_2}, \quad (\text{S25})$$

$$\dot{P}_z = -\Gamma_{\text{FB}} P_x \left(P_x - \tau\dot{P}_x + N \right) - P_y \omega_1 \cos(\omega t) - \frac{P_z}{T_1} + R_{\text{op}}. \quad (\text{S26})$$

In Eq.(S26), B_1 is small as it is a weak magnetic field applied to measure the system properties, so the transverse spin components produced by the driving field B_1 satisfy $P_x, P_y \ll 1$. Thus, the driving term $-P_y \omega_1 \cos(\omega t)$ can be neglected. When the feedback term $\Gamma_{\text{FB}} P_x$ is much smaller than P_z/T_1 and R_{op} , the nonlinear term with noise $-\Gamma_{\text{FB}} P_x (P_x - \tau \dot{P}_x + N)$ can be ignored. Then P_z reaches the steady state, corresponding to the equilibrium polarization $P_z = P_0 = R_{\text{op}} T_1$, which keeps a constant in the experiment.

We deal with Eq.(S24) and Eq.(S25) in the same way as we do with the noiseless feedback equations Eq.(S5) and Eq.(S6), we can get

$$\ddot{P}_x + \Gamma_{\text{eff}} \dot{P}_x + \omega_{\text{eff}}^2 P_x = \frac{\omega_0 \omega_1 P_0}{1 + \Gamma_{\text{FB}} P_0 \tau} \cos \omega t + \frac{\Gamma_{\text{FB}} P_0 N}{(1 + \Gamma_{\text{FB}} P_0 \tau) T_2}, \quad (\text{S27})$$

where

$$\Gamma_{\text{eff}} = \frac{1}{T_2} - \frac{\Gamma_{\text{FB}} P_0 - \frac{1}{T_2}}{1 + \Gamma_{\text{FB}} P_0 \tau}, \quad (\text{S28})$$

$$\omega_{\text{eff}} = \sqrt{\frac{\omega_0^2}{1 + \Gamma_{\text{FB}} P_0 \tau} - \frac{\Gamma_{\text{FB}} P_0 - \frac{1}{T_2}}{(1 + \Gamma_{\text{FB}} P_0 \tau) T_2}}. \quad (\text{S29})$$

Due to the consideration of noise, Eq.(S27) has an additional noise term on the right side of the equation compared to Eq.(S13) It can be found that the noise term only corrects the driving term of the damped harmonic oscillator equation and does not affect the dissipation coefficient. Therefore, the noise term of the feedback does not affect the linewidth.

Next, we analyze the correction amplitude ε of the driver term generated by the noise term. Comparing the coefficients of the two terms, we get

$$\varepsilon = \frac{\frac{\Gamma_{\text{FB}} P_0 N}{(1 + \Gamma_{\text{FB}} P_0 \tau) T_2}}{\frac{\omega_0 \omega_1 P_0}{1 + \Gamma_{\text{FB}} P_0 \tau}} = \frac{\Gamma_{\text{FB}}}{\omega_0} \times \frac{N}{\omega_1 T_2}. \quad (\text{S30})$$

In our experiment, the minimum effective linewidth is $\Gamma_{\text{eff}} = 2\pi \times 10$ Hz, the Larmor frequency $\omega_0 = \gamma B_0 = 2\pi \times 0.35$ Hz/nT $\times 2200$ nT $= 2\pi \times 7.7$ kHz, and the relaxation time $T_2 = 0.486$ ms, so

$$\frac{\Gamma_{\text{FB}}}{\omega_0} \approx \frac{2/T_2}{\omega_0} \approx \frac{2/(0.486 \text{ ms})}{2\pi \times 7.7 \text{ kHz}} \approx 0.085. \quad (\text{S31})$$

And our signal-to-noise ratio (S/N) is about 500. From Eq.(S19) we can get the magnitude of the signal in the near resonance condition $\omega = \omega_{\text{eff}} \approx \omega_0$ and the delay τ is small,

$$S = |P_x| \simeq \sqrt{\left(\frac{\frac{\omega_0 \omega_1 P_0}{2\omega_{\text{eff}}(1 + \Gamma_{\text{FB}} P_0 \tau)} (\omega_{\text{eff}} - \omega)}{(\omega_{\text{eff}} - \omega)^2 + \frac{\Gamma_{\text{eff}}^2}{4}} \right)^2 + \left(\frac{\frac{\omega_0 \omega_1 P_0}{4\omega_{\text{eff}}(1 + \Gamma_{\text{FB}} P_0 \tau)} \Gamma_{\text{eff}}}{(\omega_{\text{eff}} - \omega)^2 + \frac{\Gamma_{\text{eff}}^2}{4}} \right)^2} = \frac{\frac{\omega_0 \omega_1 P_0}{2\omega_{\text{eff}}(1 + \Gamma_{\text{FB}} P_0 \tau)}}{\sqrt{(\omega_{\text{eff}} - \omega)^2 + \frac{\Gamma_{\text{eff}}^2}{4}}} \simeq \frac{\omega_1}{\Gamma_{\text{eff}}}. \quad (\text{S32})$$

So the signal-to-noise ratio S/N is

$$\frac{S}{N} = \frac{\omega_1/\Gamma_{\text{eff}}}{N} \approx 500, \quad (\text{S33})$$

and we can obtain that

$$\frac{\omega_1}{N} \approx 500 \times (2\pi \times 10) \text{ Hz} \approx 31 \text{ kHz}. \quad (\text{S34})$$

Putting Eq.(S31) and (S34) to the expression of ε , Eq.(S30),

$$\varepsilon \approx 0.085 \times \frac{1}{31 \text{ kHz} \times 0.486 \text{ ms}} \approx 0.56\%. \quad (\text{S35})$$

It can be found that under our experimental conditions, the correction amplitude brought by noise is much smaller than that of the driving term. To be precise, because the signal-to-noise ratio of our experiment is large enough, we can safely ignore the effect of noise.

II. \mathcal{PT} -SYMMETRIC FEEDBACK IN THE OPTICAL CAVITY

Optical cavity is widely used in precision measurement experiments, and our \mathcal{PT} -symmetric feedback scheme can also be applied to the system of optical cavity to realize the linewidth narrowing. As shown in the Fig.S1, the laser is incident into the optical cavity through the phase modulator. We detect the output laser by homodyne detection, and then the detection signal is fed back to the phase modulator to modulate the phase of the input optical field. a (a^\dagger) is the annihilation (creation) operator of the light field in the Fabry-Perot cavity, satisfying the Hamiltonian $H = (\omega_c - \omega_L)a^\dagger a = -\Delta a^\dagger a$, where ω_c is the resonance frequency and ω_L is the frequency of the light field, Δ is the detuning. So the Langevin equation for the light field in the cavity is $\dot{a} = (i\Delta - \kappa)a - \sqrt{2\kappa_{\text{in}}}a_{\text{in}}$, where κ_{in} is the loss rate associated with the input coupling, κ is the total loss rate. Since the annihilation operator a can be written as two orthogonal components $a = X + iY$, the equation satisfied by the two orthogonal components X and Y is $\dot{X} + i\dot{Y} = (i\Delta - \kappa)(X + iY) - \sqrt{\kappa_{\text{in}}}(X_{\text{in}} + iY_{\text{in}})$, which can be rewritten as

$$\begin{cases} \dot{X} = -\kappa X - \Delta Y - \sqrt{2\kappa_{\text{in}}}X_{\text{in}} \\ \dot{Y} = -\kappa Y + \Delta X - \sqrt{2\kappa_{\text{in}}}Y_{\text{in}} \end{cases}. \quad (\text{S36})$$

Next, we introduce the measurement-feedback scheme. According to the input-output relation, the transmission light field satisfies $a_{\text{out}} = \sqrt{\kappa_{\text{in}}}a$. We use strong local oscillating light a_L and transmission light interference for homodyne detection, and the light intensity of the two channels after splitting through the beam splitter satisfies

$$\begin{cases} I_1 \propto (a_L^\dagger + a^\dagger)(a_L + a) = |a_L|^2 + a^\dagger a + |a_L|(e^{-i\theta}a + e^{i\theta}a^\dagger) \\ I_2 \propto (a_L^\dagger - a^\dagger)(a_L - a) = |a_L|^2 + a^\dagger a - |a_L|(e^{-i\theta}a + e^{i\theta}a^\dagger) \end{cases}, \quad (\text{S37})$$

where $\alpha_L = |a_L|e^{i\theta}$, θ is the phase of the local light. The intensity difference between the two channels is

$$I_1 - I_2 \propto 2|a_L|(e^{-i\theta}a + e^{i\theta}a^\dagger) = 4|a_L|(X \cos \theta + Y \sin \theta). \quad (\text{S38})$$

We can define

$$Q_\theta = 4|a_L|(X \cos \theta + Y \sin \theta), \quad (\text{S39})$$

so we obtain $I_1 - I_2 \propto Q_\theta$.

The signal from the photodetector is fed back to a phase modulator (e.g., electro-optic modulator, EOM) to add an additional phase ϕ to the input laser $a_{\text{in}} \rightarrow a_{\text{in}}e^{i\phi}$, where $\phi \propto I_1 - I_2$. Let η be the total conversion efficiency, including the photodetector and phase modulator conversion efficiency, we can obtain $\phi = \eta Q_\theta$. When ϕ is small, we use the Taylor expansion

$$a_{\text{in}}e^{i\phi} \approx a_{\text{in}}(1 + i\phi) = (X_{\text{in}} + iY_{\text{in}})(1 + i\eta Q_\theta) = X_{\text{in}} - \eta Y_{\text{in}}Q_\theta + i(Y_{\text{in}} + \eta X_{\text{in}}Q_\theta) \quad (\text{S40})$$

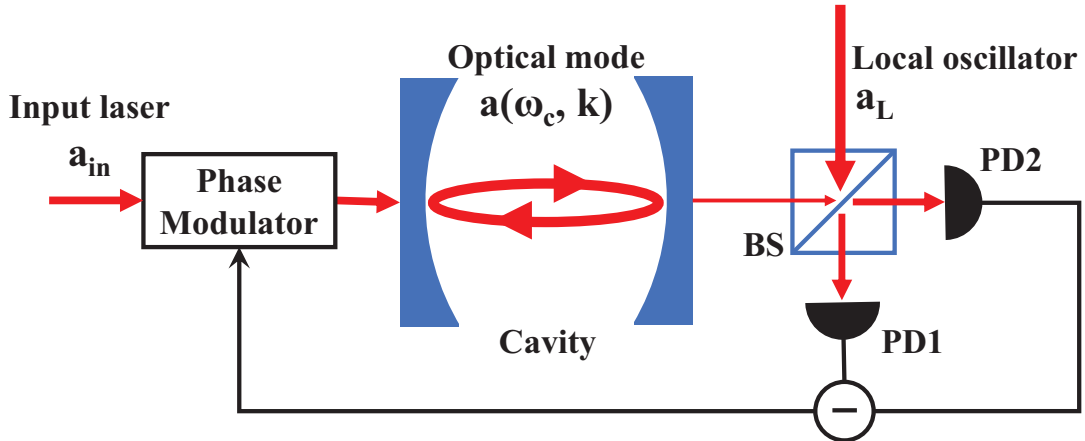


FIG. S1. Schematic diagram of an optical cavity using \mathcal{PT} feedback laser and pump laser used in the experiment. BS, beam splitter; PD, photodetector.

So the two orthogonal components of the input light are

$$\begin{cases} X'_{\text{in}} = X_{\text{in}} - \eta Y_{\text{in}} Q_{\theta} \\ Y'_{\text{in}} = Y_{\text{in}} + \eta X_{\text{in}} Q_{\theta} \end{cases} \quad (\text{S41})$$

Putting Eq.(S41) into Eq.(S36), finally we obtain that the equation of the two orthogonal components of the optical field in the cavity is

$$\begin{cases} \dot{X} = -\kappa X - \Delta Y - \sqrt{2\kappa_{\text{in}}} (X_{\text{in}} - \eta Y_{\text{in}} Q_{\theta}) \\ \dot{Y} = -\kappa Y + \Delta X - \sqrt{2\kappa_{\text{in}}} (Y_{\text{in}} + \eta X_{\text{in}} Q_{\theta}) \end{cases} \quad (\text{S42})$$

It is worth noting that the feedback breaks the symmetry of the two orthogonal components.

When the adjustable phase of the local oscillation light satisfies $\theta = 0$. From Eq.(S39), we know $Q_{\theta=0} = 4|a_L|X$. And putting it into Eq.(S42), we obtain

$$\begin{cases} \dot{X} = -\kappa X - \Delta Y - \sqrt{2\kappa_{\text{in}}} (X_{\text{in}} - 4|a_L|\eta Y_{\text{in}}X) = (-\kappa + 4\sqrt{2\kappa_{\text{in}}}\eta|a_L|Y_{\text{in}})X - \Delta Y - \sqrt{2\kappa_{\text{in}}}X_{\text{in}} \\ \dot{Y} = -\kappa Y + \Delta X - \sqrt{2\kappa_{\text{in}}} (Y_{\text{in}} + 4|a_L|\eta X_{\text{in}}X) = -\kappa Y + (\Delta - 4\sqrt{2\kappa_{\text{in}}}\eta|a_L|X_{\text{in}})X - \sqrt{2\kappa_{\text{in}}}Y_{\text{in}}. \end{cases} \quad (\text{S43})$$

This constitutes a PT-symmetric system similar to the thermal atomic system in the manuscript, with a linewidth of $2\kappa - 4\sqrt{2\kappa_{\text{in}}}\eta|a_L|Y_{\text{in}}$ in the \mathcal{PT} -symmetric phase. The conversion efficiency η can adjust the strength of feedback and realize the linewidth narrowing.

III. EXPERIMENTAL DETAILS

A. Derivation of the feedback factor

In this section, we derive the expression of feedback factor Γ_{FB} . This factor is defined as

$$B_y = -\frac{\Gamma_{\text{FB}}}{\gamma} P_x, \quad (\text{S44})$$

thus we need to derive the explicit expressions of the relation between the feedback magnetic field B_y and the measured spin polarization P_x .

Because of the spin polarization P_x , the polarization direction of the linearly polarized light rotates by an angle $\theta = k_{\theta}P_x$, where k_{θ} is the Faraday rotation coefficient of the atoms. Then we use the polarization homodyne detection to detect the Faraday rotation angle θ . The output voltage V_{PD} of the balanced photodetector has a linear relationship with the Faraday rotation angle, $V_{\text{PD}} = k_V\theta$, where k_V is the proportional coefficient. We connect the output of the balanced photodetector to the feedback loop formed by the feedback resistor R and the y -axis feedback coil R_c ($R \gg R_c$), and the current generated is $I_{\text{FB}} = V_{\text{PD}}/R$, so the feedback magnetic field is $B_y = k_I I_{\text{FB}}$, where k_I is the magnetic field generated by the coil per ampere of current. Finally, we obtain the relationship between the feedback magnetic field B_y and spin polarization P_x as

$$B_y = \frac{k_I k_V k_{\theta}}{R} P_x. \quad (\text{S45})$$

Comparing Eq. (S44) with Eq. (S45), we obtain

$$\Gamma_{\text{FB}} = -\frac{\gamma k_I k_V k_{\theta}}{R}, \quad (\text{S46})$$

which is inversely proportional to the feedback resistance R . In our experiment, we can tune the feedback factor Γ_{FB} by adjusting the feedback resistance R , with other parameters unchanged.

B. Experimental parameters

Larmor frequency $\omega_0 = \gamma B_0 = 2\pi \times 0.35 \text{ Hz/nT} \times 2200 \text{ nT} = 2\pi \times 7.7 \text{ kHz}$, relaxation time $T_1 \approx 0.6 \text{ ms}$, $T_2 = 0.486 \text{ ms}$, delay time $\tau \approx 2 \text{ us}$, optical pumping rate $R_{op} \approx 1600 \text{ Hz}$, equilibrium polarization $P_0 \approx 0.97$.

C. Energy level diagram and laser frequencies

The energy level diagrams and laser frequencies in the experiment are shown in Fig. S2. The linearly polarized probe laser power is $25 \mu\text{W}$ and its frequency is 40 GHz below the $F = 4$ to $F' = 2$ transition of the ^{133}Cs D2 line (wavelength 852 nm). The circularly polarized pump laser power is 1 mW and its frequency is on resonance with the $F = 4$ to $F' = 3$ transition of the ^{133}Cs D1 line (wavelength 894 nm).

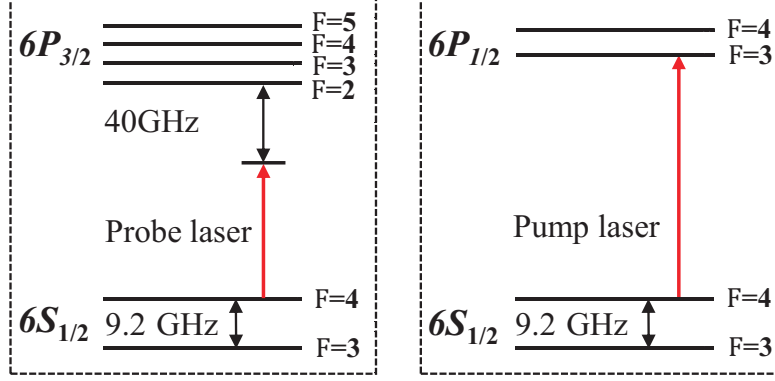


FIG. S2. Energy level diagrams of ^{133}Cs atom and the frequencies of probe laser and pump laser used in the experiment.

D. Principle of measuring the spin polarizability P_x

The far detuning linearly polarized probe light incident on the atomic vapor cell along the x direction. The right and left circularly polarized components of linearly polarized light have different refractive indices due to the spin polarization P of the atoms in the x direction. After passing through the same distance, the phase difference between left circularly polarized light and right circularly polarized light will change, thus rotating the polarization plane of probe light. This is the Faraday rotation effect.

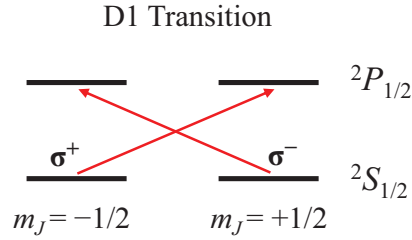


FIG. S3. Energy level diagram for D1 transition of ^{133}Cs .

For example, we consider the D1 transition of the Cs atom in the Fig.S3. The ground state of cesium has an angular momentum of $+1/2$ or $-1/2$. The transition rule determines that electrons with different orientations of spin angular momentum projection will absorb photons with different polarization states. The atom with an angular momentum of $+1/2$ only absorbs σ^- circularly polarized light, while the atom with an angular momentum of $-1/2$ only absorb σ^+ circularly polarized light. The atomic polarization (the difference in population of the ground states) makes the atomic vapor absorb light at different rates for the two different circularly polarized states, which gives rise to circular dichroism. We know that different absorbance means different refractive indices for the two circularly polarized light. This results in a phase difference between the two types of circularly polarized light emitted, which leads to a rotation of the polarization plane of the final synthesized linearly polarized light. We use a half waveplate and a polarization beam splitter to split the probe light. The intensity of the two component light fields (I_1, I_2) is detected with a balanced photodetector, and then the angle of rotation of the polarization plane of the probe light is detected by subtraction ($I_1 - I_2$). Because the rotation angle of the polarization plane of the probe light is proportional to the spin polarization in the x -direction, we can obtain the information of the spin polarization P_x .

E. Sequence diagram of the drives for two linewidth measurement schemes

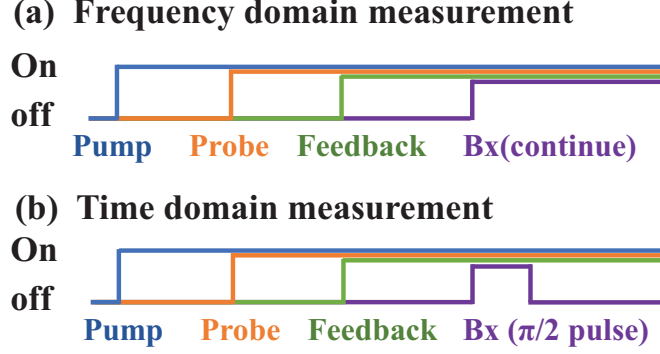


FIG. S4. (a), (b) Linewidth measurement in the frequency and time domain.

Figure S4 shows the sequence diagram of the drives for the two linewidth measurement schemes. The main difference is x -axis magnetic field B_x , which has different forms and different roles in the two measurement schemes. In the frequency domain measurement, the driving magnetic field B_x is a continuous RF magnetic field, as shown in Fig.S4 (a). We constantly change the frequency of B_x and scan through the resonance frequency of spin precession. And then we use the lock-in amplifier to demodulate the resonance lineshape and obtain the resonance linewidth. In the time domain measurement, we use a pulsed magnetic field B_x to rotate the atomic spins to the x -direction, as shown in Fig.S4 (b). Then the spins undergo Larmor precession and gradual relaxation under the action of the z -direction bias magnetic field, and the linewidth can be obtained by measuring the relaxation time.

F. Discussion of measuring magnetic field and sensitivity

The discussion of measuring magnetic field and sensitivity is divided into three parts (1) Method of measuring the magnetic field in the z -axis. (2) Definition of sensitivity and derivation of sensitivity formula (3) Experimental measurement procedures for signal-to-noise ratio S/N and sensitivity. And the reason why the feedback method improves the sensitivity is analyzed.

1. Method of measuring the magnetic field in the z -axis

There is a magnetic field B_0 to be measured in the z -direction. We apply an x -axis driving field $B_x = B_1 \cos \omega t$ and scan the frequency of the driving field ω . Then, we measure the output signal of the photodetector and use the power spectral density (PSD, $S_{\text{PSD}}(\omega)$) to represent the magnitude of the signal. According to the expression of spin polarization P_x (Eq.S19), the expression of signal power spectral density $S_{\text{PSD}}(\omega)$ can be obtained that

$$\begin{aligned}
 S_{\text{PSD}}(\omega) &= |P_x(\omega)|^2 = \left(\frac{\frac{\omega_0 \omega_1 P_0}{2\omega_{\text{eff}}(1+\Gamma_{\text{FB}}P_0\tau)} (\omega_{\text{eff}} - \omega)}{(\omega_{\text{eff}} - \omega)^2 + \frac{\Delta\omega_{\text{FWHM}}^2}{4}} \right)^2 + \left(\frac{\frac{\omega_0 \omega_1 P_0}{4\omega_{\text{eff}}(1+\Gamma_{\text{FB}}P_0\tau)} \Gamma_{\text{eff}}}{(\omega_{\text{eff}} - \omega)^2 + \frac{\Delta\omega_{\text{FWHM}}^2}{4}} \right)^2 \\
 &= \frac{\left(\frac{\omega_0 \omega_1 P_0}{2\omega_{\text{eff}}(1+\Gamma_{\text{FB}}P_0\tau)} \right)^2}{(\omega_{\text{eff}} - \omega)^2 + \frac{\Delta\omega_{\text{FWHM}}^2}{4}} \simeq \frac{\omega_1^2/4}{(\omega_0 - \omega)^2 + \frac{\Delta\omega_{\text{FWHM}}^2}{4}},
 \end{aligned} \tag{S47}$$

where $\omega_1 = \gamma|B_x|$, $P_0 \approx 1$ and $\Delta\omega_{\text{FWHM}}$ is the linewidth. The delay τ is small, so $\omega_{\text{eff}} \approx \omega_0$, $1 + \Gamma_{\text{FB}}P_0\tau \approx 1$. As shown in Fig.S5, the blue curve shows the variation of the signal power spectral density $S_{\text{PSD}}(\omega)$ with the frequency ω of the driving magnetic field. When the signal reaches its maximum, it means that the driving magnetic field frequency ω and the resonance center frequency ω_0 are equal ($\omega = \omega_0 = \gamma B_0$). According to the resonance center

frequency, the magnetic field to be measured can be calculated is $B_0 = \frac{\omega_0}{\gamma}$. And the max amplitude is

$$S_{\text{PSD}} = \frac{\omega_1^2}{\Delta\omega_{\text{FWHM}}^2}. \quad (\text{S48})$$

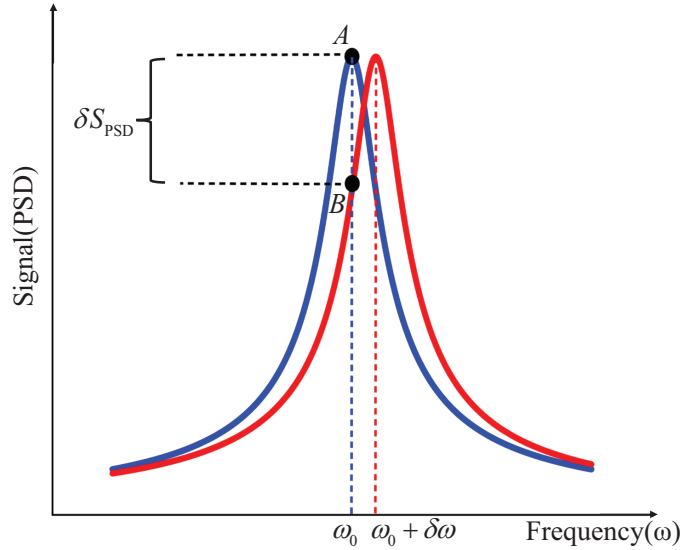


FIG. S5. Schematic diagram of the power spectral density

2. Derivation of the sensitivity formula

Suppose there is a weak change in the magnetic field to be measured $B_{\text{new}} = B_0 + \delta B$, then the new resonance frequency is $\omega_{\text{new}} = \omega_0 + \delta\omega$, and the corresponding resonance curve will be shifted, as shown in the red curve in Fig. S5. Because the frequency of the driving magnetic field remains constant ($\omega = \omega_0$) and is not equal to the new resonance center frequency ω_{new} , the signal becomes smaller, as shown by point B on the red curve. As the weak change $\delta\omega$ of the magnetic field causes the signal amplitude to change from point A to point B, the change value of the signal is δS_{PSD} . When change value of the signal δS_{PSD} and noise N_{PSD} satisfy $\delta S_{\text{PSD}} \geq N_{\text{PSD}}$, we can distinguish that the signal has changed and know that the magnetic field to be measured has changed. When $\delta S_{\text{PSD}} = N_{\text{PSD}}$, we can just distinguish that the signal has changed, and the corresponding weak change of frequency $\delta\omega$ (magnetic field δB) is our sensitivity. The value of the change in the signal can be written as

$$\delta S_{\text{PSD}} = \left| \frac{dS_{\text{PSD}}}{d\omega} \right| \delta\omega, \quad (\text{S49})$$

When weak frequency is much small than linewidth ($\delta\omega \ll \Delta\omega_{\text{FWHM}}$), we can obtain from Eq.(S47) and Eq.(S48) that

$$\left| \frac{dS_{\text{PSD}}}{d\omega} \right| = \frac{(\omega - \omega_0) \omega_1^2}{2 \left(\frac{\Delta\omega_{\text{FWHM}}^2}{4} + (\omega - \omega_0)^2 \right)^2} \approx \frac{8\omega_1^2 \delta\omega}{\Delta\omega_{\text{FWHM}}^4} = \frac{\omega_1^2}{\Delta\omega_{\text{FWHM}}^2} \frac{8}{\Delta\omega_{\text{FWHM}}^2} = \frac{8S_{\text{PSD}}}{\Delta\omega_{\text{FWHM}}^2}. \quad (\text{S50})$$

So we obtain

$$\delta S_{\text{PSD}} = \left| \frac{dS_{\text{PSD}}}{d\omega} \right| \delta\omega = \frac{8S_{\text{PSD}}}{\Delta\omega_{\text{FWHM}}^2} \delta\omega^2. \quad (\text{S51})$$

Using the criterion $\delta S_{\text{PSD}} = N_{\text{PSD}}$ for sensitivity, we obtain the expression for sensitivity $\delta\omega$ as

$$\delta S_{\text{PSD}} = \frac{8S_{\text{PSD}}}{\Delta\omega_{\text{FWHM}}^2} \delta\omega^2 = N_{\text{PSD}} \rightarrow \delta\omega = \frac{\Delta\omega_{\text{FWHM}}}{2\sqrt{2}\sqrt{S_{\text{PSD}}/N_{\text{PSD}}}}. \quad (\text{S52})$$

In the actual measurement, we input the signal to the spectrum analyzer, and the measurement result is the square root of the power spectral density (i.e., $\text{PSD}^{1/2}$). Therefore, the relationship between the signal-to-noise ratio S/N obtained in the actual measurement and the power spectral density signal-to-noise $S_{\text{PSD}}/N_{\text{PSD}}$ is

$$\frac{S}{N} = \sqrt{\frac{S_{\text{PSD}}}{N_{\text{PSD}}}}. \quad (\text{S53})$$

Putting Eq.(S53) into Eq.(S52), we obtain the measurement sensitivity as

$$\delta\omega = \frac{1}{2\sqrt{2}} \frac{\Delta\omega_{\text{FWHM}}}{S/N}. \quad (\text{S54})$$

The corresponding magnetic field sensitivity is

$$\delta B = k_F \frac{\Delta\omega_{\text{FWHM}}}{\gamma} \frac{1}{S/N}, \quad (\text{S55})$$

where $k_F = \frac{1}{2\sqrt{2}}$. It is worth noting that our calculation is a sensitivity analysis of the system operating very close to resonance. When the detected magnetic field change does not satisfy $\delta\omega \ll \Delta\omega_{\text{FWHM}}$, it will affect $|\frac{dS_{\text{PSD}}}{d\omega}|$ and modify the coefficient k_F . However, the scaling rule $\delta B \propto \Delta\omega_{\text{FWHM}}/(S/N)$ still holds.

3. Experimental measurement procedures for signal-to-noise ratio and sensitivity

According to Eq.(S55), we need to measure the linewidth and the signal-to-noise ratio at resonance to calculate the sensitivity. The method of measuring linewidth in the time or frequency domain has been described in detail in the main text, so the following section focuses on the measurement of signal-to-noise ratio.

We send the signal of the photodetector to the spectrum analyzer for measurement. First, we do not add the driving magnetic field B_x to obtain the power spectral density of noise, the maximum value of the noise is N , as shown by the black dashed line in Fig.S6(a). Then, we apply the driving magnetic field B_x and scan to the resonance frequency. The peak value at the resonance of the power spectral density represents the signal strength S , so we can obtain the signal-to-noise ratio S/N . With or without feedback, the signal-to-noise ratio is measured in the same way. The black curve in the Fig.S6(a) is the measurement result without feedback, and the red curve is the result with feedback. The signal strength with feedback (red solid line) is significantly greater than the signal strength without feedback (black solid line) but the feedback also brings an increase in noise (red dashed line), so the signal-to-noise ratio does not improve. We can measure the linewidth and signal-to-noise ratio for different feedback coefficients and calculate the sensitivity improvement factor compared to no feedback case according to Eq.(S55), as shown in Fig. S6(b). Although the signal-to-noise ratio is not improved, the feedback scheme can narrow the linewidth by up to 48 times, which can still bring a maximum of 22 times improvement according to the formula Eq.(S55).

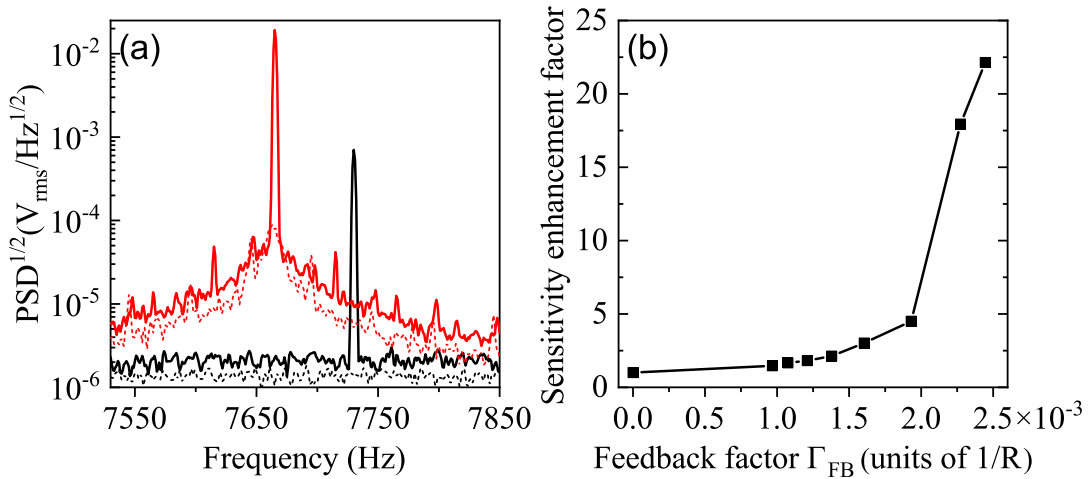


FIG. S6. (a) Square root of power spectral density ($\text{PSD}^{1/2}$) for feedback resistance $R = 409 \Omega$ (red curves) and without feedback (black curves). The solid (dashed) curves are the results in the presence (absence) of driving magnetic field B_x . (b) Sensitivity enhancement factor of the M_x magnetometer as a function of the feedback factor.